Electronic Supplementary Information

Melting of a single ice microparticle on exposure to focused near-IR laser beam to yield a supercooled water droplet

Shuichi Hashimoto*[a] and Takayuki Uwada[b]

[a] Advanced Engineering Course, NIT Gunma College, 580 Toriba-machi, Maebashi, Gunma 371-8530, Japan,

[b]Department of Chemistry, Josai University, 1-1 Keyakidai, Sakado, Saitama 350-0295, Japan.

S1. Propagation of droplet crystallization.

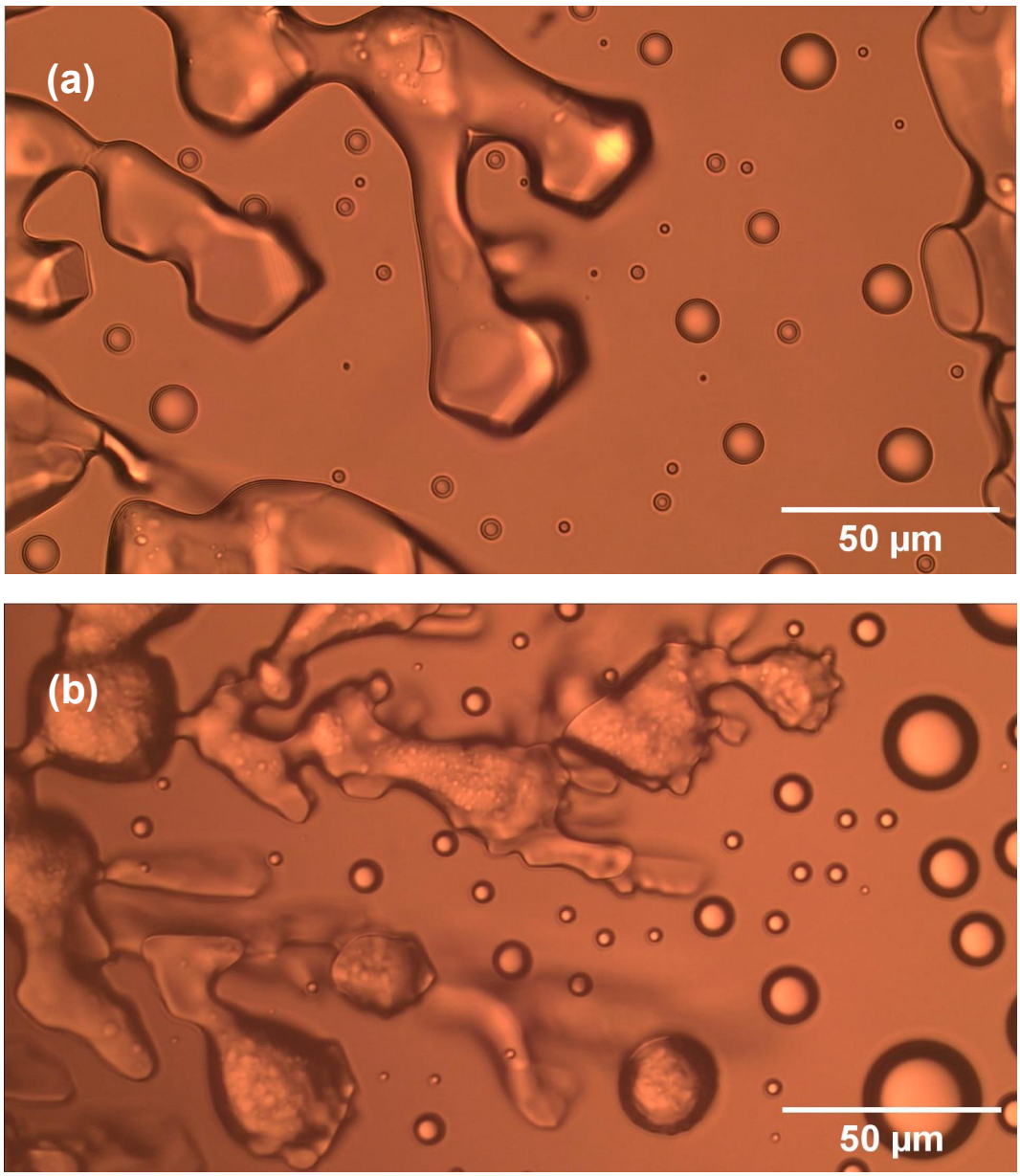

Figure S1 (a), (b) During the ice crystallization, dynamic growth was observed by capturing droplets, forming connected and large structures.

S2. Raman spectra of a water droplet at various ambient temperatures.

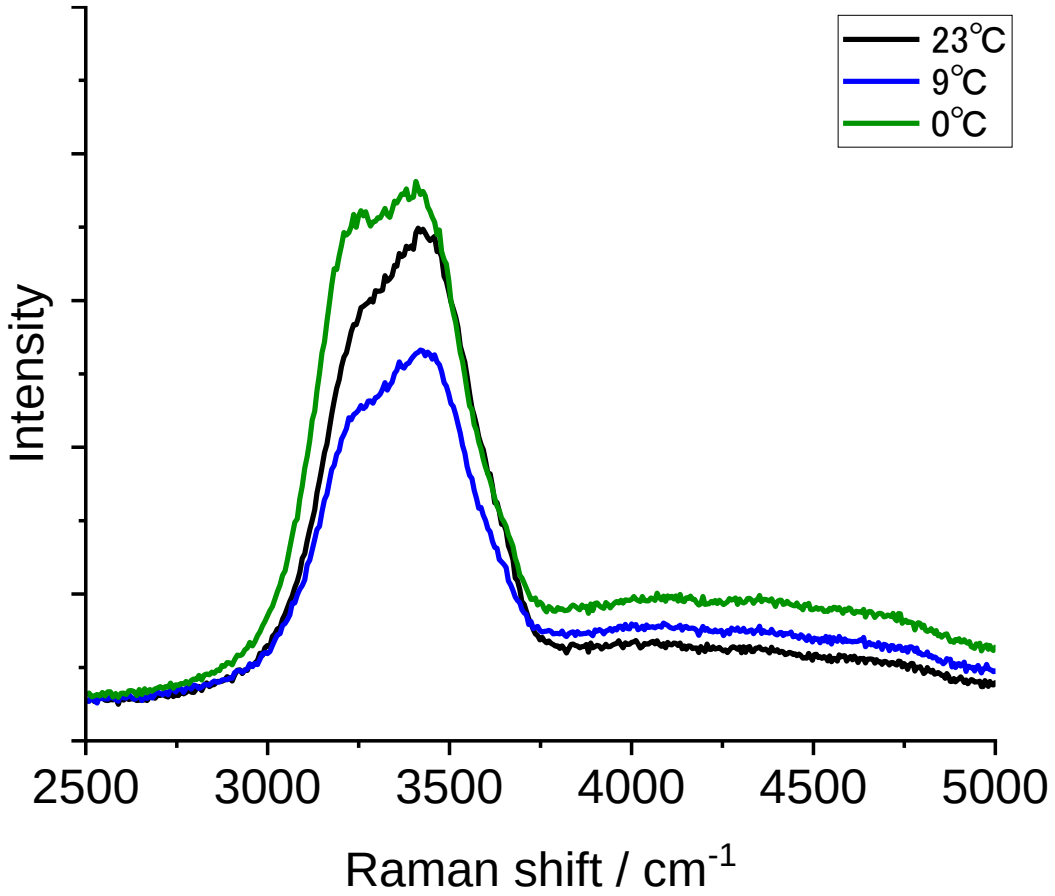

Figure S2 Comparison of Raman spectral shapes were made at three temperatures: 23, 9, 0°C.

S3. In-situ Raman spectra for Figure 6.

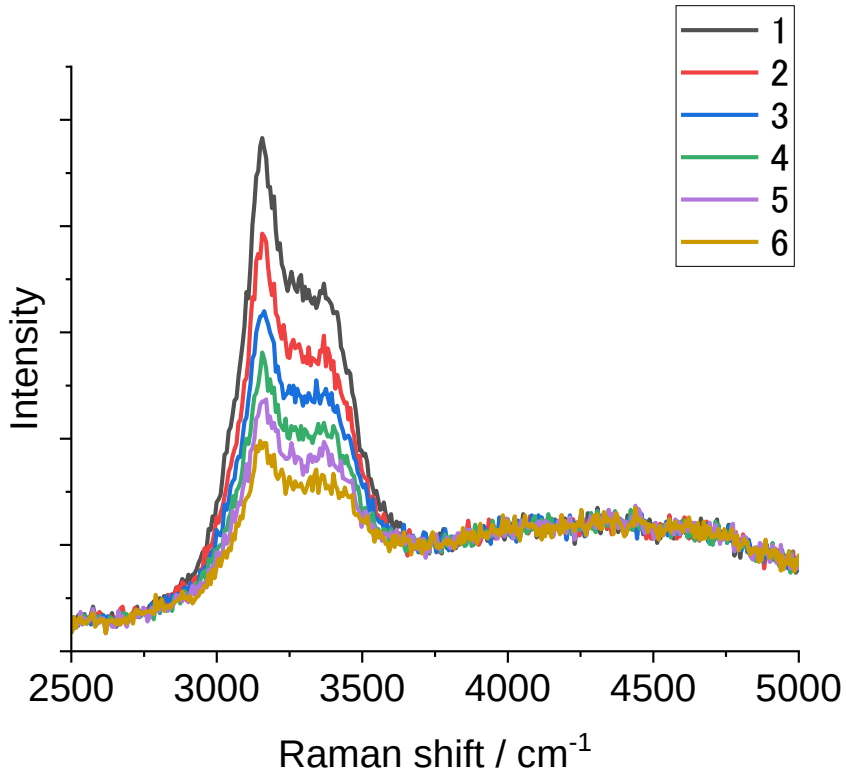

Figure S3 Single particle Raman spectral evolution associated with Figure 6 on exposure to laser illumination (1064 nm, 50mW) of a single ice particle at −15°C. Raman spectra were acquired every 10s. The spectral numbers represent the bin numbers of the spectral accumulation (1, 0-10 s; 4, 30-40 s; 5, 40-50 s; 6, 50-60 s).

S4. Numerical simulation using COMSOL.

A commercial finite-element mode solver, COMSOL Multiphysics Ver. 6.0 (http://www.comsol.com), was used for temperature estimation under illumination of a focused laser beam on an ice microparticle (MP). The schematic illustration of simulation geometry built for COMSOL is shown in Figure S3a. All the elements: the ice MP (30-μm diameter sphere or hemisphere), air layer, and glass substrates (upper and lower) were included in the model based on the experimental configuration. At the center of the ice MP, we placed an elliptical spot representing a laser spot. The lengths of the minor and major axes for the laser spot were determined by the full width at half maximum (FWHM) intensity of the laser spot on the basis of lateral and axial resolutions[1].

$$\text{(lateral resolution)}\ \frac{0.51\lambda}{\mathrm{NA}} \qquad \text{(axial resolution)}\ \frac{2n\lambda}{\mathrm{NA}^2}$$

where λ is the wavelength of a laser (1064 nm), n is the refractive index of the surrounding air (1.0), and NA is the numerical aperture of the objective lens (0.6). Physical properties of ice, air, and glass substrates such as thermal conductivity, viscosity, and heat capacity, and density were taken from the COMSOL Material library[2].

The heat generation by laser illumination was assumed to be triggered by the absorption of light at the laser spot, i.e., the elliptical spot in ice MP. The absorption coefficient of ice (water), α, at 1064 nm was taken from the literature[3], 0.14 cm^{-1}, and the heat generated at the laser spot, Q, was calculated with the following equation[4].

$$Q = I\alpha$$

where I represents the intensity of the laser beam, which is defined as the average of the incident laser power at the elliptical volume that acted as a heat source. Next, we calculated the temperature distribution in a chamber using the heat transfer module[5]. As an initial condition, the temperature distribution in the model was assumed to be uniform and equal to 253 K. The heat is continuously generated upon the laser illumination and is transferred to the surrounding, resulting in an increased steady-state temperature distribution throughout the chamber. Time-dependent heat transfer in the model is expressed by the following equation[5]:

$$\rho C_P \left(\frac{\partial T(\mathbf{x},t)}{\partial t} + \mathbf{u}(\mathbf{x},t) \cdot \nabla T(\mathbf{x},t) \right) = \nabla \cdot \left(k \nabla T(\mathbf{x},t) \right) + Q(t)$$

where T(**x**, t) is temperature at arbitrary position **x** at time t, ρ is the mass density, C_P the specific heat capacity at the constant pressure, **u**(**x**, t) the fluid velocity vector, k the thermal conductivity of the system at the position **x**, and Q(t) is the energy deposition term. In this case, the temperature elevation in the ice MP is supposed to exceed a phase transition temperature of ice at 273.15 K. Thus, we considered the latent heat of fusion and change of physical properties at the phase transition temperature. The detail of the phase change is described in the application note "Phase Change" released by COMSOL[6]. In the calculation, the value of latent heat of fusion, 333.5 kJ kg^{-1} and that of the transition interval, 10 K were used. The temporal change of the temperature at the top of the ice is shown in Figure S3b. Because of the heat transfer from the laser spot, the temperature of ice is increased with time but we can find a small step around 270 K from 0 to 0.2 s, indicating the heat dissipation by the latent heat of fusion. The temperature reached a steady-state approximately at 3 s after the laser illumination. The maximum temperature was calculated as 314 K.

For hemispherical ice MP, which is akin to the observed droplet shape, we calculated the heat transfer from the laser spot and temperature elevation in the same manner. The temperature distribution map around the hemispherical ice upon laser illumination is shown in Figure S5a. The laser power was set to 50 mW. At the top of the ice, the temperature reached 297 K, which is lower than that of spherical ice. This temperature suppression occurred from heat dissipation to the glass substrate because of a greater contact area.

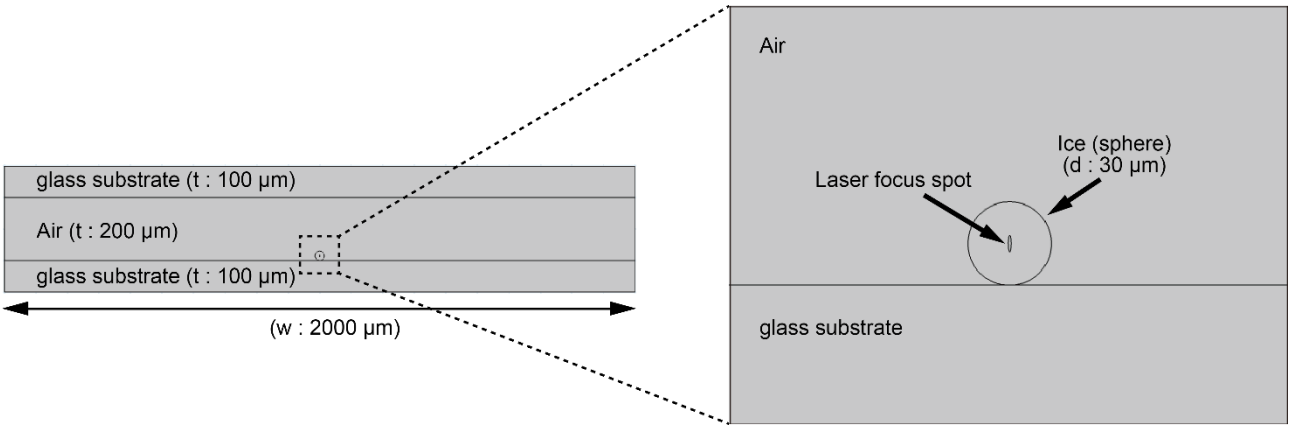

Figure S4 (a) Schematic illustration of the simulation geometry.

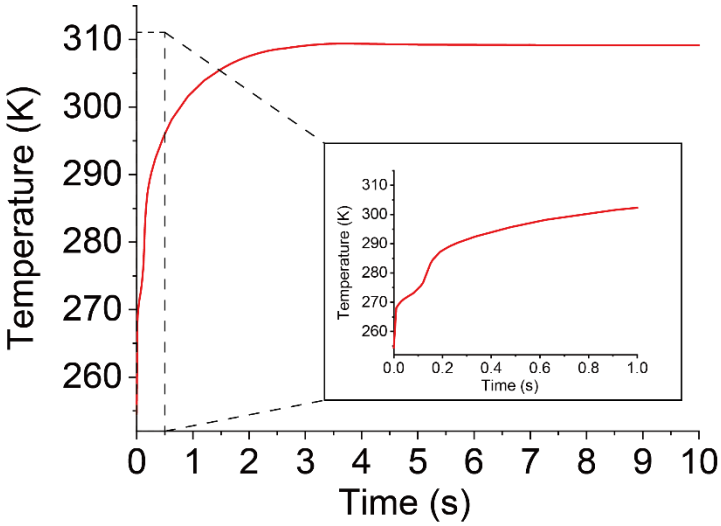

Figure S4 (b) Temporal evolution of the temperature at the top of ice in the model shown in Fig. S 4a.

S5. Calculated temperature distributions in hemispherical particle and bulk ice.

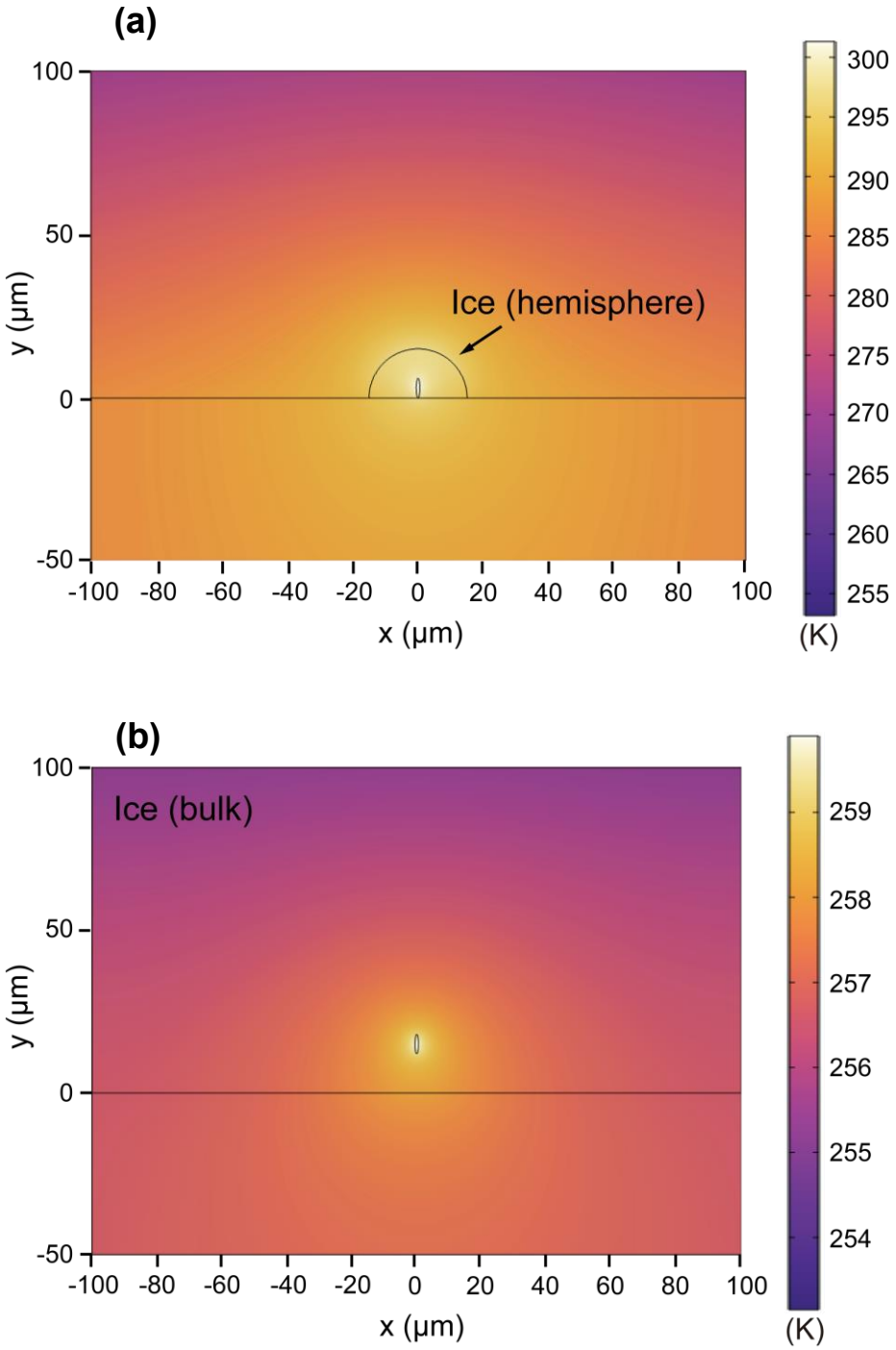

Figure S5 (a) Temperature distribution for d=30 μm hemispherical ice particle supported on a substrate, (b) Temperature distribution in 200×200×200 μm^3 cubic ice that represents bulk ice. Max temperatures obtained are 301 K in a and 260 K in b.

S6. Observation of slow sublimation without melting of ice particle at low laser intensities.

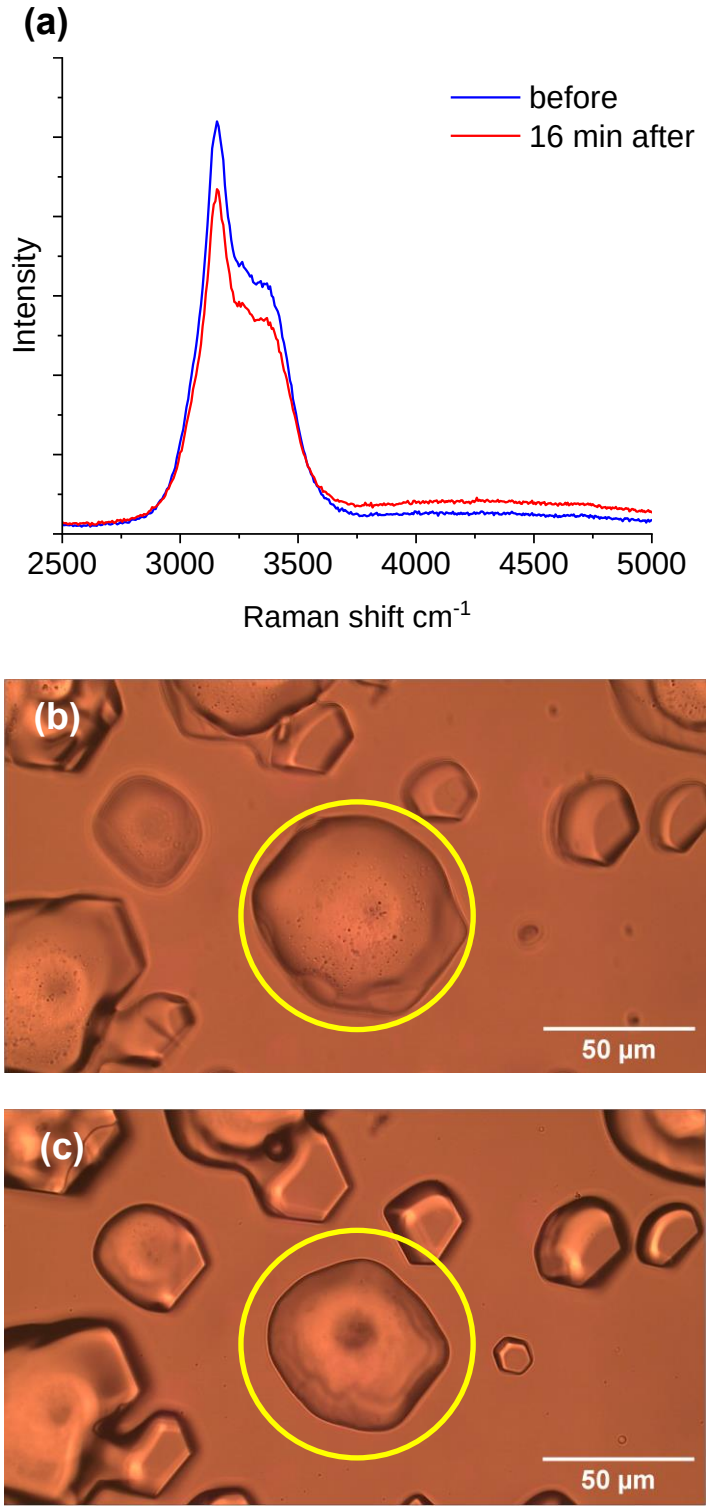

Figure S (a) Raman spectral change of ice before (b, ~70 μm) and after (c, ~50 μm) 1064-nm laser illumination with an intensity of 20 mW for 16 min (environmental temperature: −13°C.). Each spectrum was acquired after 10 s of exposure. Raman spectra were unchanged during the illumination that caused a gradual particle size reduction.

S7. Observation of evaporation from ice particle at high laser intensities.

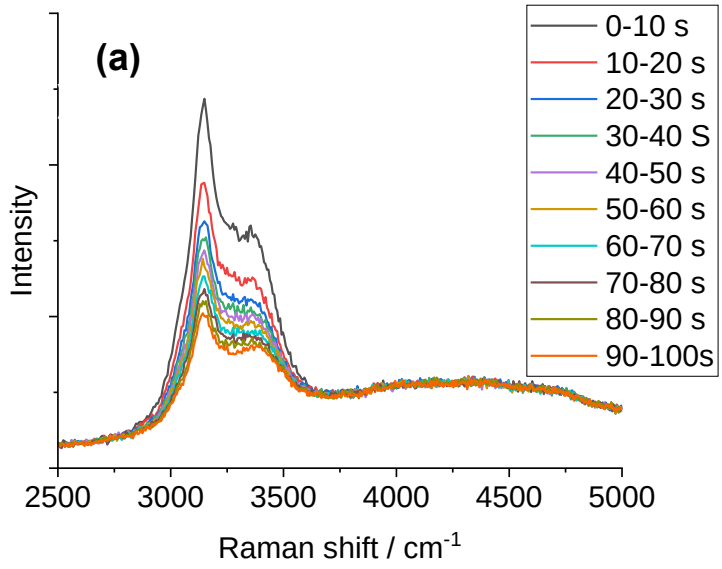

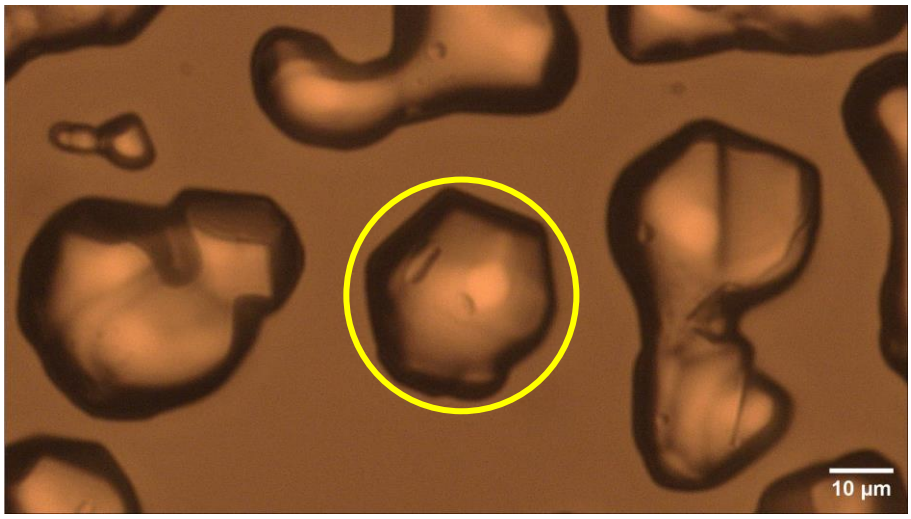

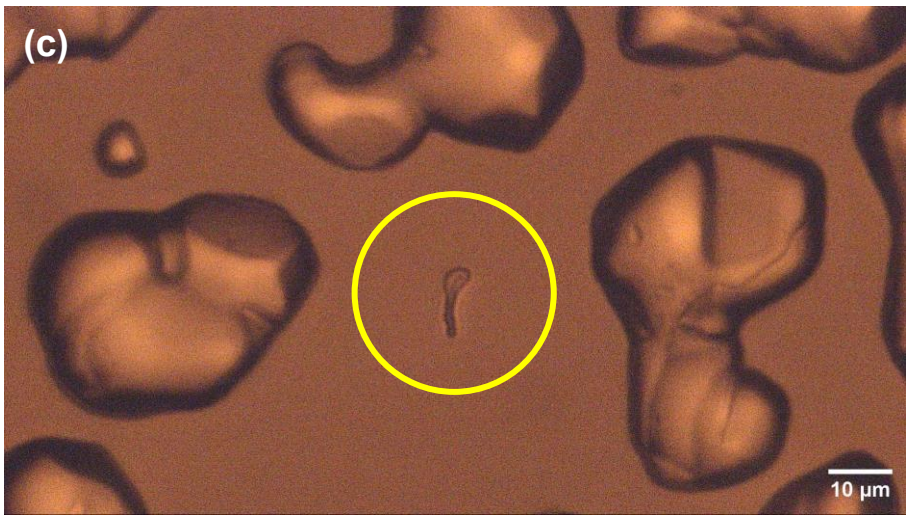

Figure S (a) In-situ Raman spectra of ice before (b, ~30 μm) and after (c) 1064-nm laser illumination with an intensity of 200 mW for 100 s (environmental temperature: −10°C.). Raman spectral shapes were unchanged during the illumination that caused a fast particle size reduction.

S8. Laser-power and particle diameter-dependent temperature distribution on water droplets.

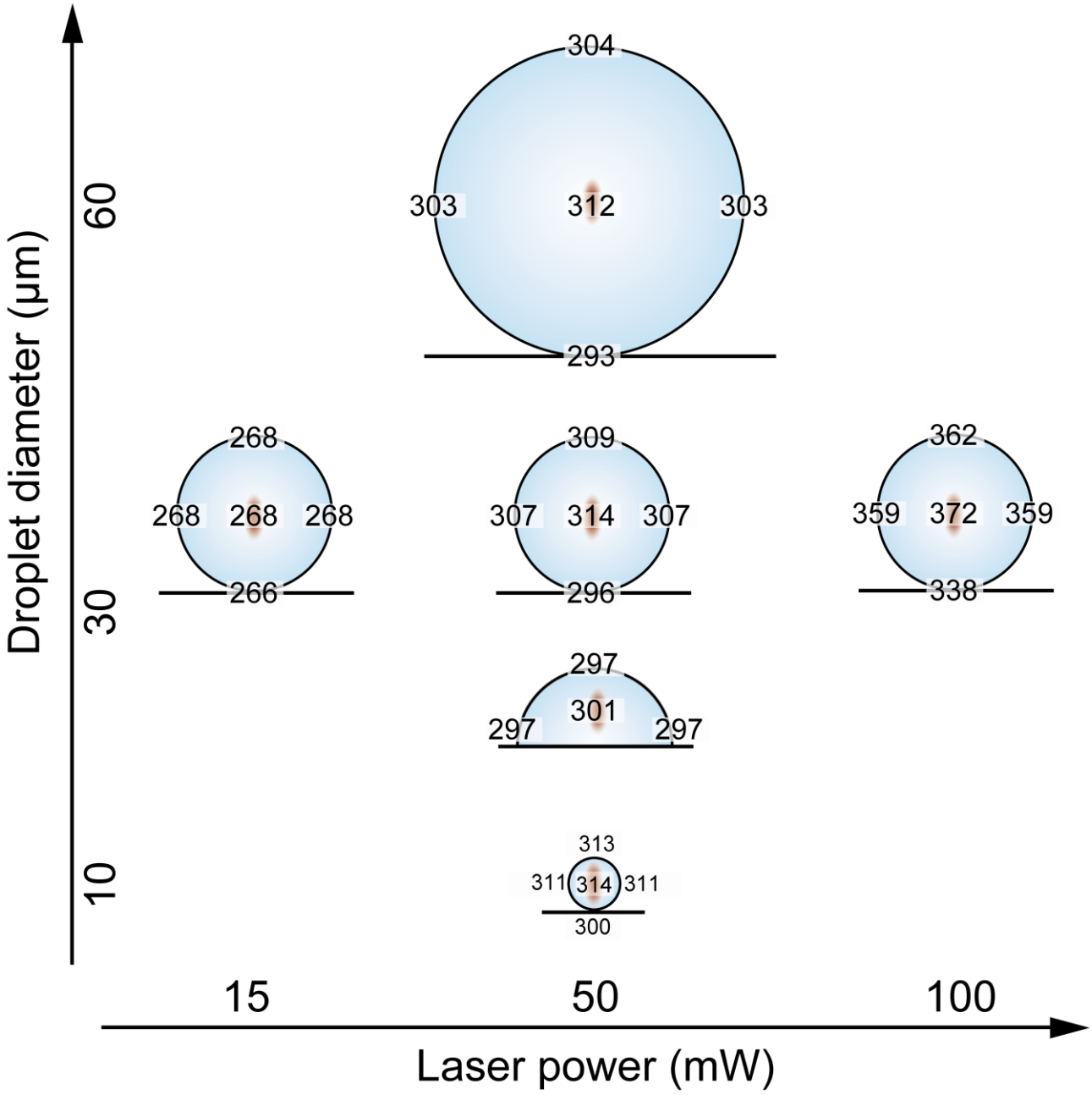

Figure S Calculated temperature (K) distributions using COMSOL for droplets with various diameters under laser illumination. Initial condition is that ice particles are supported on a glass substrate at 253 K (−20°C).

S9. Raman spectral changes observed for bulk ice on photothermal heating of gold nanoaggregates. [7]

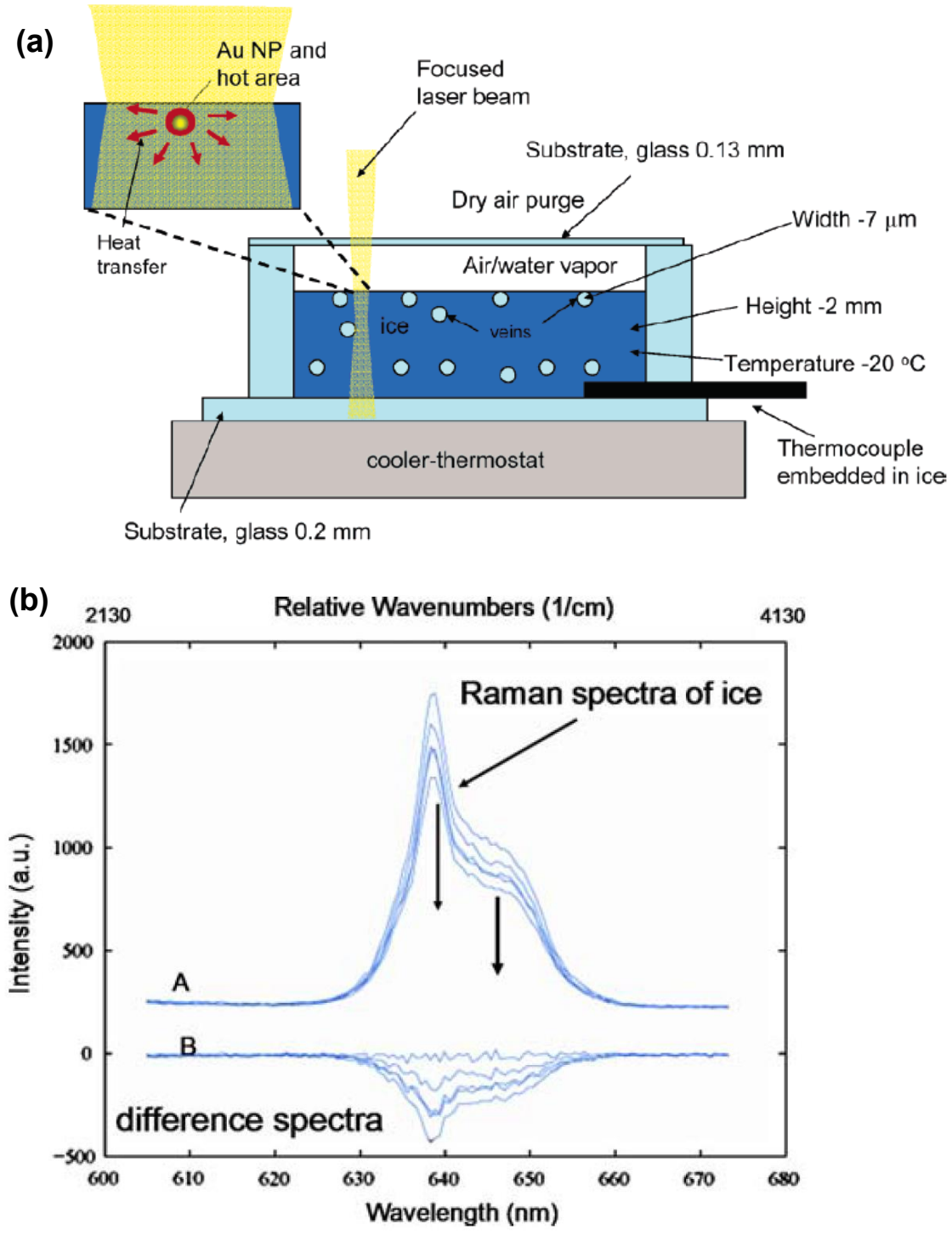

Fig S6 (a) Experimental well (3-mm in diameter and 3-mm deep) that contains ice embedded AuNPs, showing 50-nm Au NP excited with a focused laser beam and heat transfer to the ice matrix.

(b) Experimental Raman spectral evolution of ice on 532-nm laser irradiation.

References

1. J. Trägårdh, K. Macrae, C. Travis, R. Amor, G. Norris, S. H. Wilson, G.-L. Oppo, G. McConnell, *J. Microscopy*, 2015, **259**, 66–73.
2. https://www.comsol.com/blogs/using-the-material-libraries-in-comsol-multiphysics/
3. J. G. Erwin, F. G. Peterman,; Schmidt, C.F. Laser-Induced Heating in Optical Traps. *Biophys. J.* 2003, 84, 1308–1316.
4. S. Ito, T. Sugiyama, N. Toitani, G. Katayama, H. Miyasaka, Application of Fluorescence Correlation Spectroscopy to the Measurement of Local Temperature in Solutions under Optical Trapping Condition. *J. Phys. Chem.* B 2007, **111**, 2365-2371
5. https://www.comsol.com/heat-transfer-module
6. https://www.comsol.jp/model/phase-change-474
7. H. H. Richardson, Z. N. Hickman, A. O. Govorov, A. C. Thomas, W. Zhang, M. E. Kordesch, Thermooptical properties of gold nanoparticles embedded in ice: characterization of heat generation and melting. *Nano Lett*. 2006, **6**, 783–788.